Chapter 6

Radiation Safety Aspects of Linac Operation with Bremsstrahlung Converters

Matthew Hodges and Alexander Barzilov

Additional information is available at the end of the chapter

http://dx.doi.org/10.5772/intechopen.71317

Abstract

This chapter provides a discussion of radiation safety aspects of operation of electron linear accelerators equipped with bremsstrahlung converters. Electron accelerators with 3, 6, 9 and 15 MeV electron beams are discussed. High-energy photon and photoneutron production during linac operation was analyzed using Monte Carlo methods. Radiation dose rates for different configurations of linacs were evaluated and compared with experimental results.

Keywords: linac, bremsstrahlung, photoneutrons, MCNPX, dose rate, radiation safety

1. Introduction

A linear accelerator (linac) is a system that increases kinetic energy of charged particles using oscillating electric potentials along the line of a beam of the particles (e.g., electrons, protons, ions). Within a few meters, it is possible for 10 keV electrons to be accelerated by the RF linac to up to 20 MeV [1]. Accelerators including linacs have found use in a variety of applications including radiotherapy [2, 3], physics [4, 5], isotope production [6], cargo inspection [7, 8], and non-destructive assay [9, 10].

In inspection systems and non-destructive assay applications, electron linacs are used to generate high energy photons that can penetrate objects under scrutiny. The accelerated electrons are bombarded onto a target composed of high-Z material. The incident electrons are deflected by electric field of the electron cloud of atomic nuclei of the target material, losing kinetic energy that is converted into the bremsstrahlung (or *braking radiation*). The bremsstrahlung photons produced by a linac are characterized by their energy distribution (the quantity of photons produced at specific energies). Linacs generate photons which have endpoint

energy equal to the maximum energy of the electrons in the beam impinging on the target. In a 10 MeV linac, the bremsstrahlung has continuous spectrum from 0 up to 10 MeV photons. These photons are typically focused into a desired beam shape by the use of collimators (e.g., fan beams, conical beams). The beam of collimated photons is then used for a variety of applications including imaging, radiotherapy, the production of medical isotopes, or to perform an active assay of unknown materials. The photon flux is the number of photons passing through a defined area (e.g., 1 cm^2) per unit of time.

If the energy of an incident photon is greater than that of the neutron binding energy of material it interacts with, a neutron can be produced through the (γ,n) reaction. At photon energies greater than 10 MeV, the (γ,n) reaction will take place within materials that commonly compose the accelerator facility structures [11].

Radiation safety aspects are very important in operation of linacs with bremsstrahlung converters. To describe the effects of high-energy photons and photoneutrons produced by the linac on materials and personnel, it is necessary to quantify the amount of energy deposited by radiation when it interacts with matter. The term *dose* describes the amount of energy deposited by radiation within the material, while the *biological dose* describes the energy deposited in a living tissue. The biological dose equivalent is the dose multiplied by a quality factor Q used to express the biological damage variation between the different radiation types. The quality factor has the following values: $Q = 1$ for x-rays, gamma rays, or beta particles; $Q = 20$ for alpha particles and heavy ions including fission fragments; $Q = 10$ for neutrons and for high-energy protons [12].

The international system (SI) unit of dose is the *Gray* (Gy) and is equal to the absorption of 1 joule of energy by 1 kg of material. The *Rad* is equal to 1/100 Gy. The *Rem* is equal to the product of the absorbed dose and the quality factor. The terms *dose rate* and *biological dose rate equivalent* are used to describe the respective doses received per unit time. Once radiation fluxes in an environment have been characterized, the dose rates can be determined through the use of the energy-dependent flux-to-dose conversion factors for a specific radiation type. Several flux-to-dose conversion factors have been established (i.e., ANSI/ANS 6.1.1-1997 [13]).

Two Varian linacs—the M6 and K15 models equipped with bremsstrahlung converters—with 3, 6, 9 and 15 MeV electron beams were studied for operation at the shielded building. Radiation doses due to the linac operation in different configurations were analyzed using Monte Carlo modeling and experimental measurements.

2. Characterization of radiation generated by linac

It is important to understand the radiation generated during the linac operation and how that radiation is transported throughout the building in order to determine the location specific doses. Estimating the location specific dose rates within the building allows for verification of

building safety measures, as well as help to evaluate expected dose rates at different distances from the linac structure which is vital for future research projects which may involve the irradiation of different sample materials.

Computational modeling is widely used to study behavior of complex systems. Models typically use numerous variables that characterize the system being studied. Simulation is performed by the adjustment of these variables and the subsequent observation of the outcome of the system. Computational modeling is often used as a first step in providing an estimation of parameters for a proposed experiment. When possible, model results should be validated against experimental measurement in order to determine the accuracy of simulations. Computational modeling is a valuable tool that allows for studying the effects of changing experimental parameters prior actually performing these experiments or designing radiation facilities, and for estimating their safety characteristics.

The Monte Carlo methods form a broad class of stochastic algorithms that proved successful in a variety of disciplines including genetics [14], space physics [15] and economics [16]. While problems might be solvable using deterministic methods, Monte Carlo methods utilize repetition of random sampling to arrive at a numerical result. With respect to nuclear science and radiation transport, Monte Carlo codes are used to track particle interactions with matter over a wide range of energies in a complex geometry [17, 18]. The computational modeling in this study is based on the Monte Carlo technique using the general purpose Monte Carlo N-Particle Transport software suite developed by Los Alamos National Laboratory—MCNP5 [19] and MCNPX [20] codes.

2.1. Monte Carlo model of linac

The accelerator facility at University of Nevada, Las Vegas was used as a representative building to study radiation safety aspects of operation of M6 and K15 linacs. The facility consists of an entry room, a shielding maze, and an accelerator bay. The control room is located south of the facility building itself, and is home to the operating controls of the linac as well as radiation detection equipment.

The ceiling in the facility is 20 cm thick concrete, with the walls and floors being 15 cm thick; also composed of concrete. The entry room is a large open space that measures approximately 11 m by 10 m. The shielding maze is formed by two walls of concrete bricks that serve to minimize the radiation doses in the entry way that are due to radiation emitted from the linac in the accelerator bay. The southern shield maze wall is 4 m long, 87 cm thick and the north wall is 7.5 m long and 117 cm thick. Both shielding walls are 2.5 m tall and extend almost completely to the ceiling. The scheme of the facility is shown in **Figure 1**.

The material compositions of the internal facility structures were taken from reference [21]. The M6 linac and K15 linac were modeled using different MCNP codes. The model of the M6 linac was run using MCNP5 with the ENDF/B-VII cross sections (denoted by the ".70c" identifier in MCNP5) at room temperature. The model of the K15 linac used the MCNPX code because it could not be run in MCNP5 due its lacking of photonuclear physics and the proper cross section library.

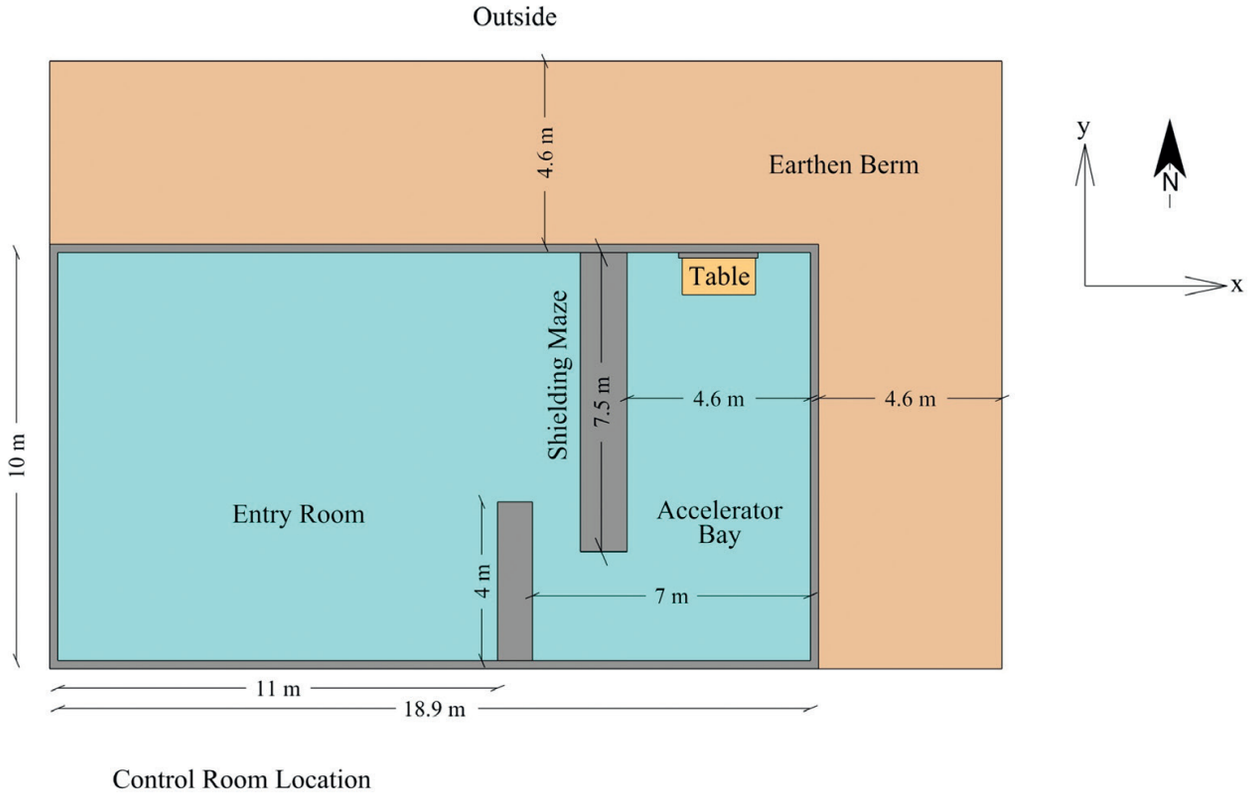

Figure 1. Accelerator facility layout.

2.2. Linac source definition

The computational models of the M6 and K15 linacs start with the simulation of an electron beam impinging upon the linac target head. The target head geometries and comprising material differ between the two linacs, and were each modeled according to the Varian specifications. In order for a computational model to produce precise results, it is necessary to accurately describe the source term. The source definition (SDEF) card is used to define the particle transport required within the MCNP model. An example of the MCNP5 input to define the electron source term is shown below:

sdef x d1 y 0 z d2 erg = d3 par 3 vec 0 1 0 dir 1.

sp1 −41 0.065 0.

sp2 −41 0.065 0.

sp3 −41 0.120 6.

The "mode p e" card was used to include photon and electron transport in the model. The "phys:p" card was used to include the production of bremsstrahlung by electrons. The source was defined to be a 1.3 mm electron pencil beam traveling in the *y*-direction. The *x* and *z* directions of the electron beam followed distributions *d1* and *d2* to use the built-in Gaussian probability (denoted by −41) for spatial coordinates extending 0.65 mm in both directions. The *erg* value specified the energy of the electrons in the beam using distribution *d3* to set the

Gaussian-type function centered on 6 MeV. The *par* value of the source card was set to 3 to specify an electron source and the *vec* and *dir* values were set to <0 1 0 > and 1 respectively, to specify the direction of the electron beam along the *y*-axis. The source term was checked to ensure the Gaussian nature of both the spatial coordinates and energy distribution (see **Figure 2** that shows 3 and 6 MeV cases for the M6 linac).

The K15 linac's source term was defined similarly, except the average energy in the *sp3* was set as 15 MeV (or 9 MeV in the low energy mode). Furthermore, neutrons were added to the "mode" card. The "phys:p" card default values must be modified to account for photonuclear production in the model. The *ispn* value (4th entry) on the "phys:p" card must be changed from 0 (default) to either −1 (the analog photonuclear particle production) or 1 (the biased photonuclear particle production). Additionally, the *fism* value (7th entry) of the "phys:p" card was set to 1 to enable the LLNL fission model (as opposed to the default ACE model). The LLNL model was used because the ACE model does not account for prompt photofission gamma rays [22].

2.3. Computational determination of radiation flux

To evaluate the bremsstrahlung photons produced within the respective linac target heads, it was necessary to determine their angular distribution and energy spectra. Thin (0.01 cm), concentric ring surfaces were set in the model in 1 cm behind the linac target head. F4 tallies (track length estimates of the cell flux) were set within each ring surface allowing for the determination of the x-ray flux at 10° increments off the centerline (see **Figure 3**). Two hundred equally spaced energy bins were used at each tally in order to determine the energy distribution of photons. The relative error associated with each bin in an MCNP tally (corresponding to one standard deviation) is given by the inverse square root of the number of source particles contributing to that tally. The MCNP suggestion is below 10% error for F4 tallies.

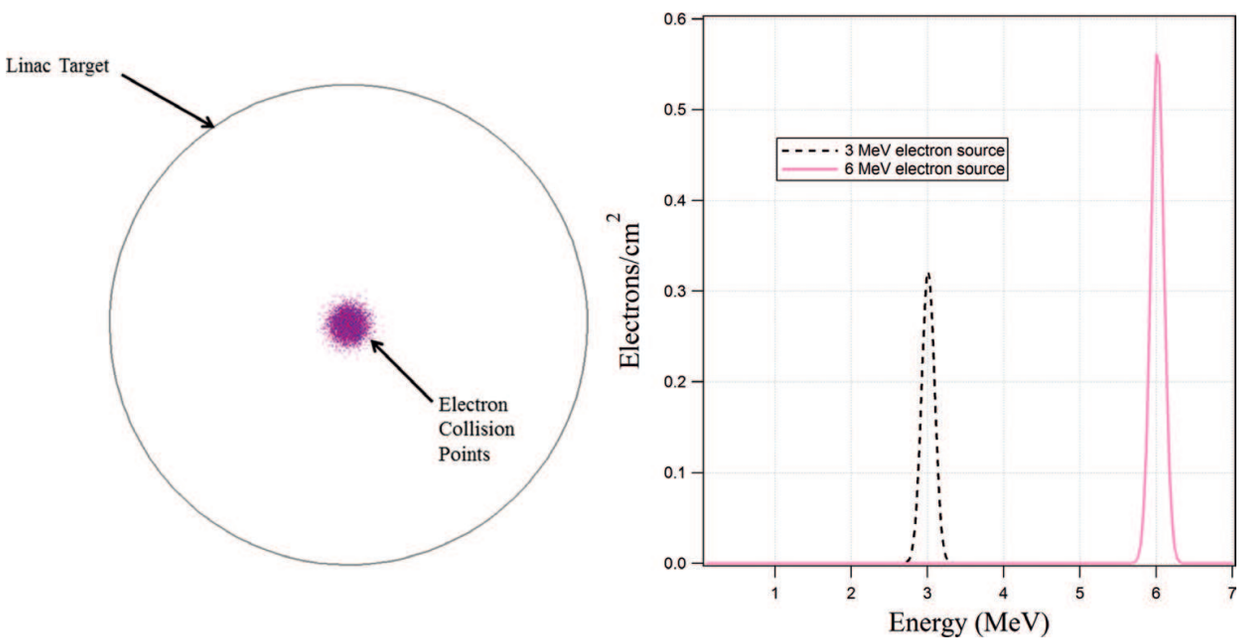

Figure 2. Spatial distribution (left) and energy distribution (right) of electrons on the M6 linac target.

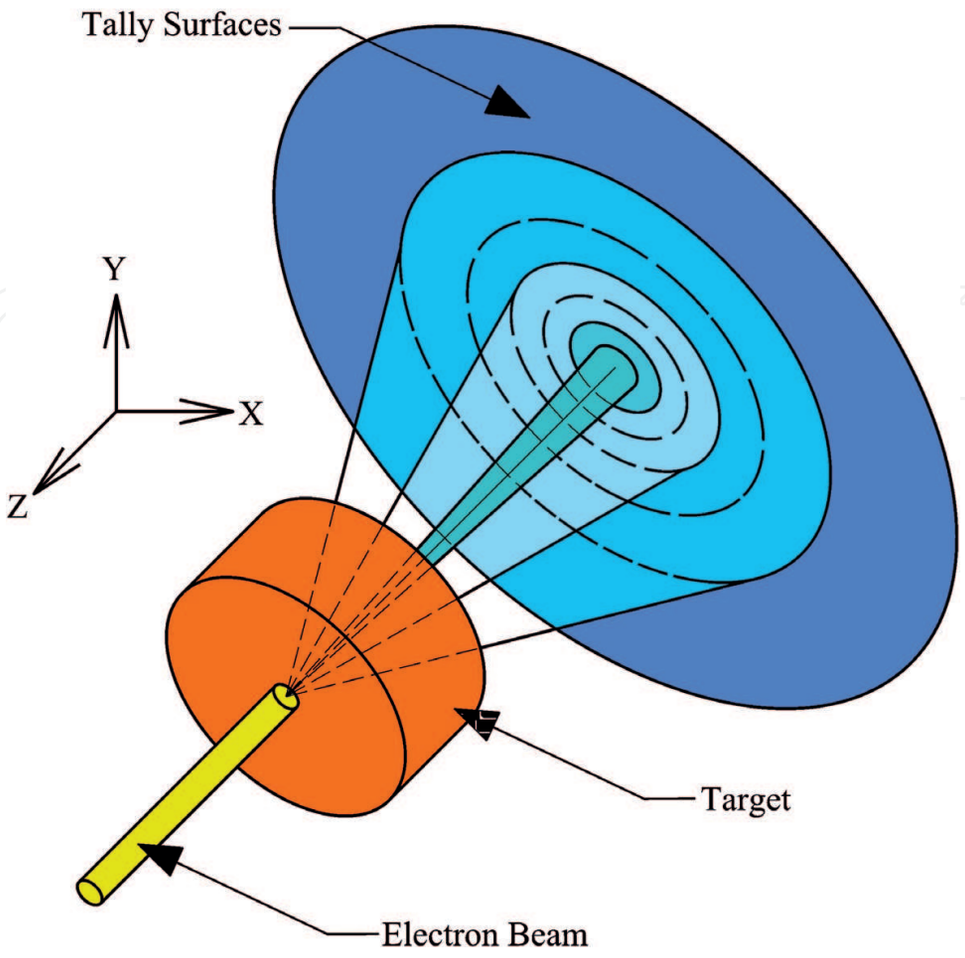

Figure 3. Schematic of tallying of bremsstrahlung angular distribution.

A mesh tally was used to determine the x-ray fluxes and dose rates due to operation of the M6 linac within the accelerator facility at the height of the fan beam (1.2 m above the floor). The FMESH card was used to determine the photon fluxes at 7.54 cm intervals in the x and y directions throughout the building. The dose energy (DE) and dose function (DF) cards were used in the MCNP5 model to convert the computed photon fluxes into dose rates by using the ANSI/ANS 6.1.1-1977 photon flux-to-dose rate conversion factor [13]. In addition to the FMESH tally, F5 tallies (flux estimators at a point) surrounded by the *dxtran* spheres were used to determine the dose rates at specific points within the facility. Moreover, the dose rate was measured by an ion chamber intrinsic to the M6 linac.

A mesh tally was similarly used to determine the photon and neutron dose rates within the accelerator facility for operation of the K15 linac, but the mesh tally syntax used in MCNPX differs from that used in MCNP5. In MCNPX, the TMESH tally with RMESH (denoting a rectangular mesh) was used to determine the dose rates throughout the building at the same spatial intervals as used in the M6 linac model. The dose rate conversions are handled in MCNPX within the RMESH by using the keyword DOSE and specifying the *ic* value as 20 (corresponding to the ANSI/ANS 6.1.1-1977 flux-to-dose factors) for both photons and neutrons.

The "NPS" card was used to set the particle history cutoff. Once the number of simulated particle histories exceeds the number specified by the NPS card, the MCNP model stops running and generates an output file, from which the results can be analyzed. Some models can take several days or weeks to complete depending on a computer, the intricacies of the model's physics, the cutoff value, and the type and energy of particles in the simulation. Charged particles (i.e., electrons) have large numbers of interactions due to the long-range Coulomb force whereas neutral particle interactions are defined by infrequent isolated collisions [23]. As such, simulations involving charged particle transport take longer to complete than those without a charge.

2.4. Determination of electron current on linac targets

The MCNP tally results are normalized per a starting particle. As the MCNP models of linacs in this study began with the simulation of electron transport, it was necessary to determine the number of electrons per second in the beam impinging the target in order to acquire quantifiable values for photon flux and dose rates. The M6 and K15 linacs utilize pulsed electron bunches to produce the bremsstrahlung radiation. As the electron current is not constant, it is required to determine the DC averaged current for each linac.

The voltage of a single pulse of the electron beam on the M6 linac target head was measured using a Teledyne Lecroy oscilloscope. The single pulse voltage waveform was converted to single pulse current by dividing by the resistance (50 Ω), determining the total area under the curve and multiplying by the frequency (156.555 Hz) to obtain a total DC averaged electron current of 3.4×10^{14} electrons per second. The electron current values for the K15 linac were provided by Varian.

3. Radiation fluxes and dose rates during linac operation

3.1. Bremsstrahlung spectra

The spectra of x-rays generated in the bremsstrahlung converter within the M6 linac were determined for the low (3 MeV electron beam) and high (6 MeV electron beam) energy operation modes with the results shown in **Figure 4**. The largest photon fluxes occur within 10° of the central axis of the linac target and decrease with increasing the angle. The trend of decreasing flux with increasing energy is apparent in both of the computed spectra. There is an order of magnitude difference between the fluxes at each angular interval between the two M6 operation modes. This is due to the greater likelihood that higher energy electrons will produce bremsstrahlung radiation with higher energy within the linac target. The error associated within each energy bin in the bremsstrahlung spectra are less than the MCNP recommended value of 10% for F4 tallies.

The radial variation of the photon flux within the conical segments was tested. Thin cylindrical cells were placed radially at 30° intervals throughout the conical segment. F4 tallies were set in each of these cells with the results showing that the flux at each radial location had similar

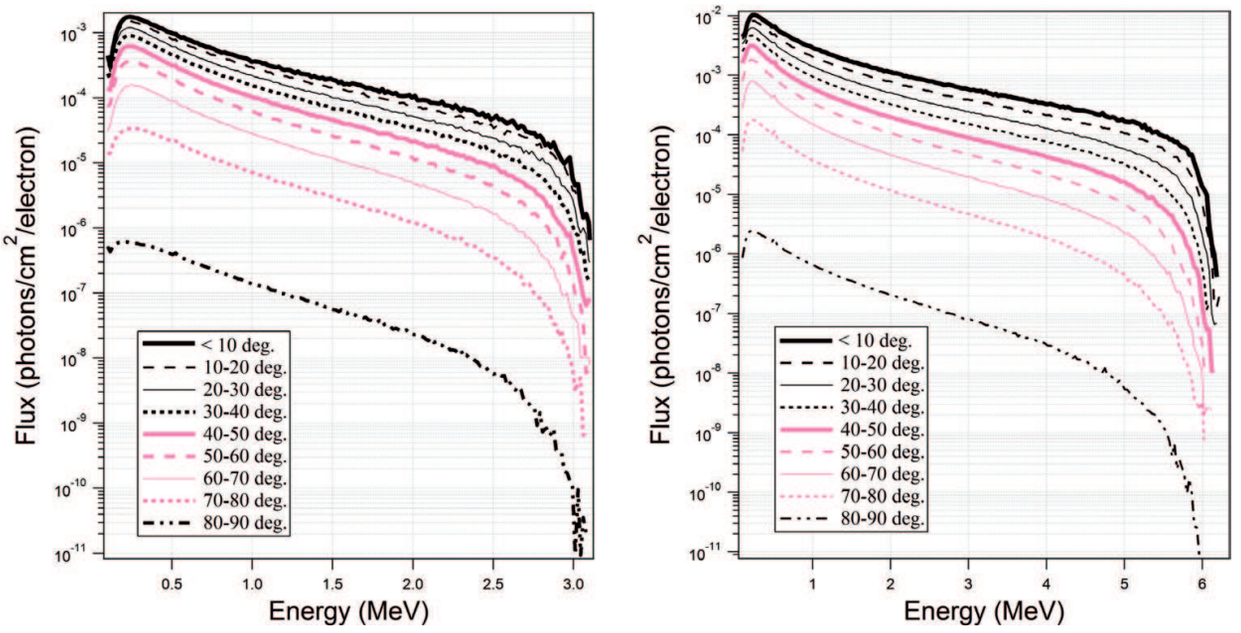

Figure 4. M6 linac: bremsstrahlung photon spectra, 3 MeV (left) and 6 MeV (right) incident electrons.

spectral distributions. Thus, the x-ray source exhibited the radial symmetry within conical segments. As the computational results for the flux are normalized to one starting particle (electron), they must be multiplied by the number of particles (described previously) in order to evaluate the photon flux generated by the target.

The bremsstrahlung spectra for the K15 linac were computationally determined for the low (9 MeV) and high (15 MeV) energy operation modes with the results shown in **Figure 5**. A total

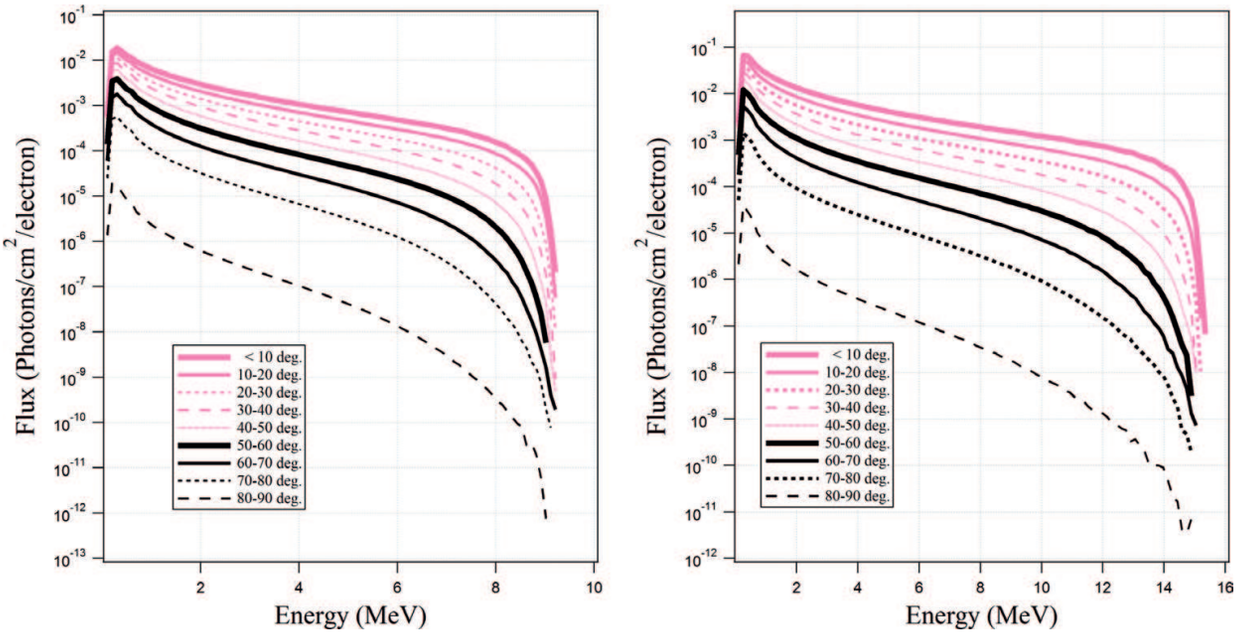

Figure 5. K15 linac: bremsstrahlung photon spectra, 9 MeV (left) and 15 MeV (right) incident electrons.

of 500 million particle histories were used in the simulation to ensure that the error associated with each of the 100 equally spaced energy bins was below the 10% recommended by MCNP for F4 tallies. As was the case with the M6 linac, the largest photon fluxes occur within 10° of the center line of the linac target and decrease with increasing outward angle. In both operating modes, at energy around 1 MeV, the photon fluxes are generated nearly three orders of magnitude larger within an angle of 10°, than they are at angles greater than 80°. This flux ratio increases to five orders of magnitude for 8 MeV photons. There is about an order of magnitude difference between the fluxes at each angular interval between the two K15 linac operation modes.

3.2. Electron energy cutoff

The MCNP5 models used to determine the M6 photon spectra were run using an NPS value of 10^8 starting electrons in order to minimize the error in each energy bin. Difficulty exists in determining the proper balance between minimizing computational time while maintaining satisfactory results. In order to reduce the computational time in this study, the suitability of using energy cutoff cards was investigated. Care must be taken when using energy cutoff cards as their use affects the underlying physics, resulting in the halting of particle interactions occurring under this energy threshold. In some instances, this may remove certain reactions from happening in the model or may modify results incorrectly beyond that which was originally determined. Results obtained from models using energy cutoffs should be compared against those without using energy cutoffs in order to make an accurate assessment as to whether their use is acceptable. The M6 bremsstrahlung spectra were determined using electron energy cutoffs of 0.001 (default), 0.01, 0.1 and 1.0 MeV with an NPS of 10^7 electrons. The results of the photon fluxes using the default and 1.0 MeV energy cutoffs for the first four energy bins are shown in **Table 1**.

The results showed that using the electron cutoff energy of 1.0 MeV in the MCNP5 model provided in photon flux values of above 70% similarity to the original results at all angle intervals within the first energy bin (below 0.1 MeV). In the second energy bin (between 0.1 and 0.16337 MeV), the average similarity rose to around 85% and by the third bin 90%. Above the third energy bin, average similarities between the two models rose to 95%. It was found that as the energy increased, so too did the similarity between model results for photon fluxes. Above the 1 MeV electron cutoff, the photon fluxes were identical. The computational time (rounded to the nearest minute) for running the MCNP5 model with the default energy cutoff (0.001 MeV) was 8876 min; 866 min with 0.01 MeV cutoff; 134 min with 0.1 MeV cutoff; and 43 min with 1 MeV cutoff. Using an electron energy cutoff of 1 MeV reduces the time required to complete the MCNP5 run by 99.5%; therefore, this cutoff value was used in this study.

3.3. Radiation environment during operation of M6 linac

While it is important to evaluate the dose rates within the facility due to operation of the M6 linac under normal operating conditions, it is also important to understand the dose rates for other possible scenarios. As future research activities may require the M6 linac usage without the fan beam collimators, it is necessary to evaluate the dose rates within the building under such operating conditions. Further, an understanding of the maximum dose rates achievable

	E (MeV)	< 10°	10–20°	20–30°	30–40°	40–50°	50–60°	60–70°	70–80°	80–90°
Default	0.1	4.47E − 03	4.11E − 03	3.39E − 03	2.52E − 03	1.59E − 03	7.91E − 04	2.76E − 04	5.31E − 05	8.56E − 07
Cut-off	0.1	3.58E − 03	3.28E − 03	2.68E − 03	1.97E − 03	1.24E − 03	6.00E − 04	2.02E − 04	3.70E − 05	6.24E − 07
Default	0.16337	1.29E − 02	1.12E − 02	9.29E − 03	7.04E − 03	4.87E − 03	2.75E − 03	1.15E − 03	2.57E − 04	3.58E − 06
Cut-off	0.16337	1.14E − 02	9.99E − 03	8.17E − 03	6.22E − 03	4.17E − 03	2.34E − 03	9.64E − 04	2.13E − 04	2.95E − 06
Default	0.22673	2.00E − 02	1.60E − 02	1.24E − 02	9.29E − 03	6.25E − 03	3.65E − 03	1.56E − 03	3.48E − 04	4.70E − 06
Cut-off	0.22673	1.88E − 02	1.51E − 02	1.17E − 02	8.50E − 03	5.66E − 03	3.25E − 03	1.40E − 03	3.07E − 04	4.12E − 06
Default	0.2901	2.05E − 02	1.59E − 02	1.18E − 02	8.56E − 03	5.78E − 03	3.35E − 03	1.48E − 03	3.37E − 04	4.53E − 06
Cut-off	0.2901	2.00E − 02	1.51E − 02	1.13E − 02	8.07E − 03	5.35E − 03	3.10E − 03	1.35E − 03	3.05E − 04	4.07E − 06

Table 1. Electron energy cutoff study: photon flux results.

due to the M6 linac operation helps to characterize safety features within the building as well as evaluate the effectiveness of the linac shielding. The normal operation mode of the M6 linac includes the use of tungsten collimator pieces to shape the emitted x-rays into a horizontal fan beam at a height of 1.2 m above the floor. Lead shielding was used within the linac assembly to minimize dose rates to the sides and rear.

Three M6 linac configurations were studied: (1) normal operation configuration with collimators and shielding; (2) collimators were removed, but shielding left intact; (3) both collimators and shielding were removed (the maximum dose rate scenario). For each linac configuration, the FMESH tally was used to determine the overall dose rate footprint while F5 tallies were used to determine the dose rates at specific building locations. Comparison of the specific dose rates under differing M6 configurations allowed for determination of the effectiveness of the collimator pieces and linac shielding in reducing dose rates throughout the building. The MCNP5 models do not incorporate the earthen berm to the north east of the facility. This allows for studying the shielding effectiveness of the concrete wall alone. In actuality, the earthen berm completely envelops the northern, northeastern and eastern walls of the facility.

The computed dose rates due to the M6 linac operation under the normal operation configuration, in both high and low energy mode are shown in **Figures 6** and **7**. It was found that dose rates within the accelerator facility are higher when the M6 linac is operated in the high energy mode than when it is operated in the low energy mode. This is due to higher energy photons being produced (the endpoint energy of 6 MeV as opposed to 3 MeV) as well as larger fluxes of lower energy photons. For example, the computed flux of 1 MeV photons

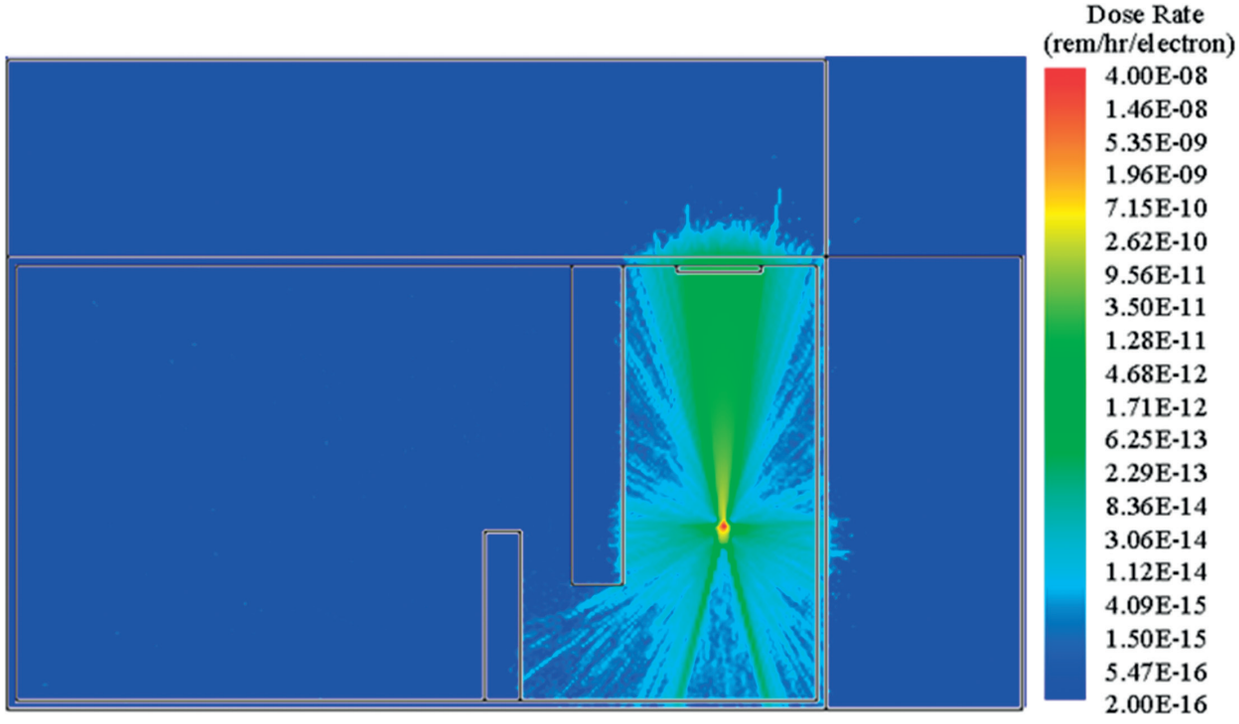

Figure 6. M6 linac in the normal operation configuration: dose rates for 6 MeV electron beam.

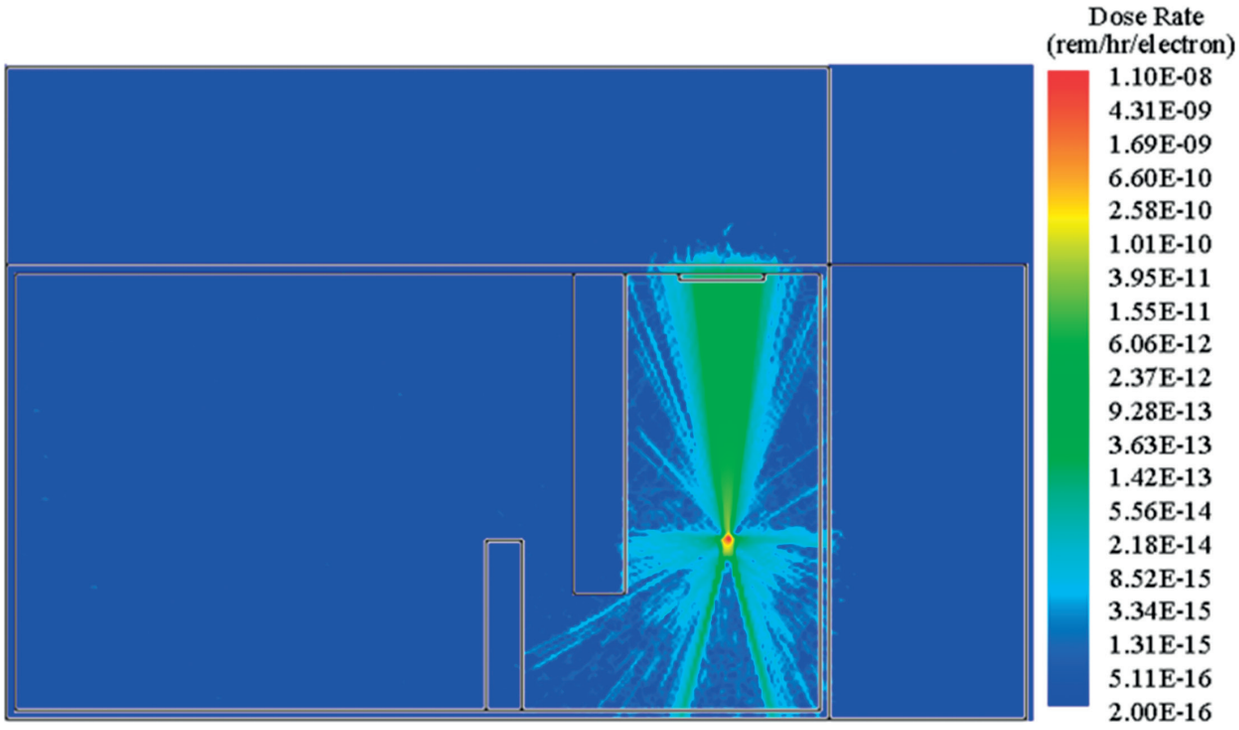

Figure 7. M6 linac in the normal operation configuration: dose rates for 3 MeV electron beam.

produced in high energy mode is an order of magnitude larger than when in low energy mode. The dose rates are largest directly in front of the linac, where the collimated beam is located. The fan shape is visible in both energy modes, with dose rates being higher in high energy mode. In both energy modes, the shielding maze minimizes the dose rates within the accelerator entry way.

Under certain conditions (i.e. production of photoneutrons using a low-threshold neutron converter or irradiation of large samples), the M6 linac may be used without the tungsten collimator pieces. As these collimator pieces attenuate the majority of emitted photons in all but the specific beam shape, the removal of these pieces leads to an increase in the photon fluxes and dose rates expected not only in the northern half of the facility, but throughout the building. The emitted photons will no longer take the shape of a fan beam, but rather a cone with dimensions according to the collimator cavity. The expected dose rates due to the M6 linac operation without collimators are shown in **Figures 8** and **9**. Similar to the configuration 1, the dose rates in the accelerator facility when the M6 linac is operated without collimators are higher when it is operated in the high energy mode. It was found that the dose rates within the northern half of the accelerator bay are greatly increased when the collimators are removed. In addition, it was determined that the dose rates in the entry way (0.259 ± 0.0020 rem/h) were larger than they were in the configuration 1 (0.0004 ± 0.00002 rem/h).

Determination of the dose rates within the accelerator facility for operation of the M6 without shielding and collimator materials constitutes the "worst case scenario," or maximum possible dose rates achievable (see **Figures 10** and **11**). It is important to evaluate these dose rates in order to help validate safety measures for the facility. Removing the

http://dx.doi.org/10.5772/intechopen.71317

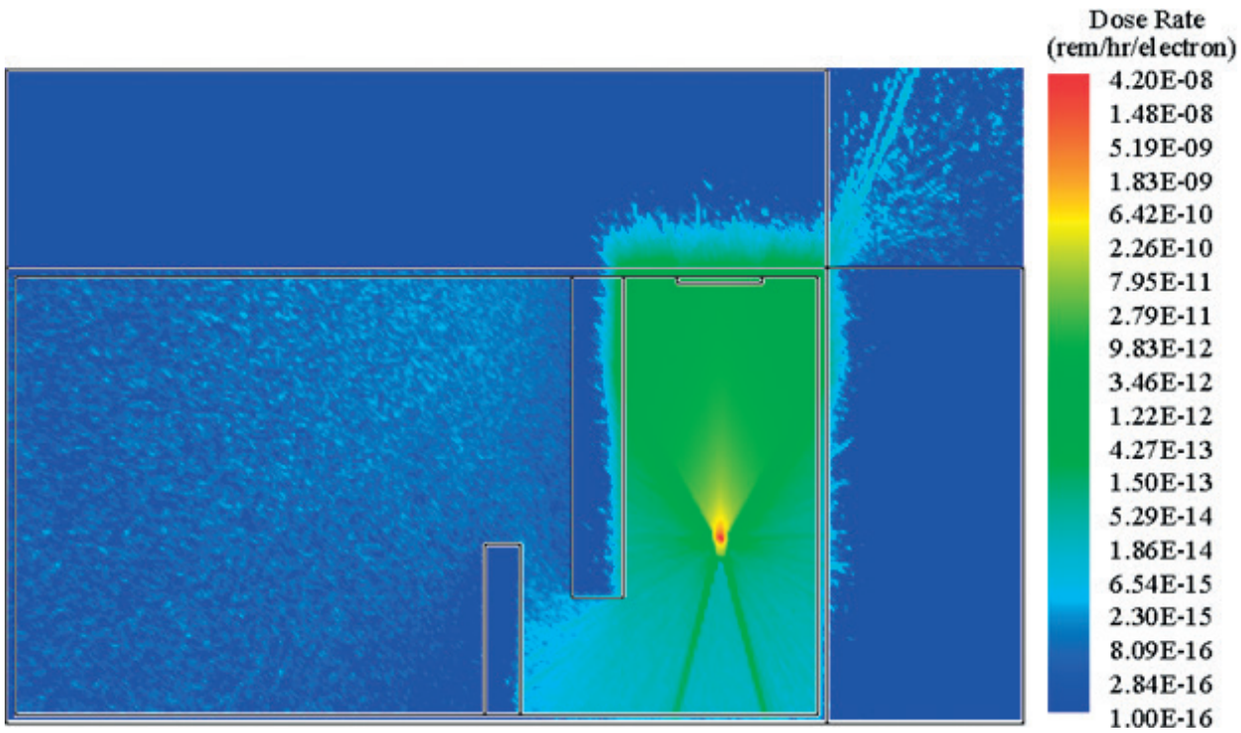

Figure 8. M6 linac in the 2nd configuration: dose rates for 6 MeV electron beam.

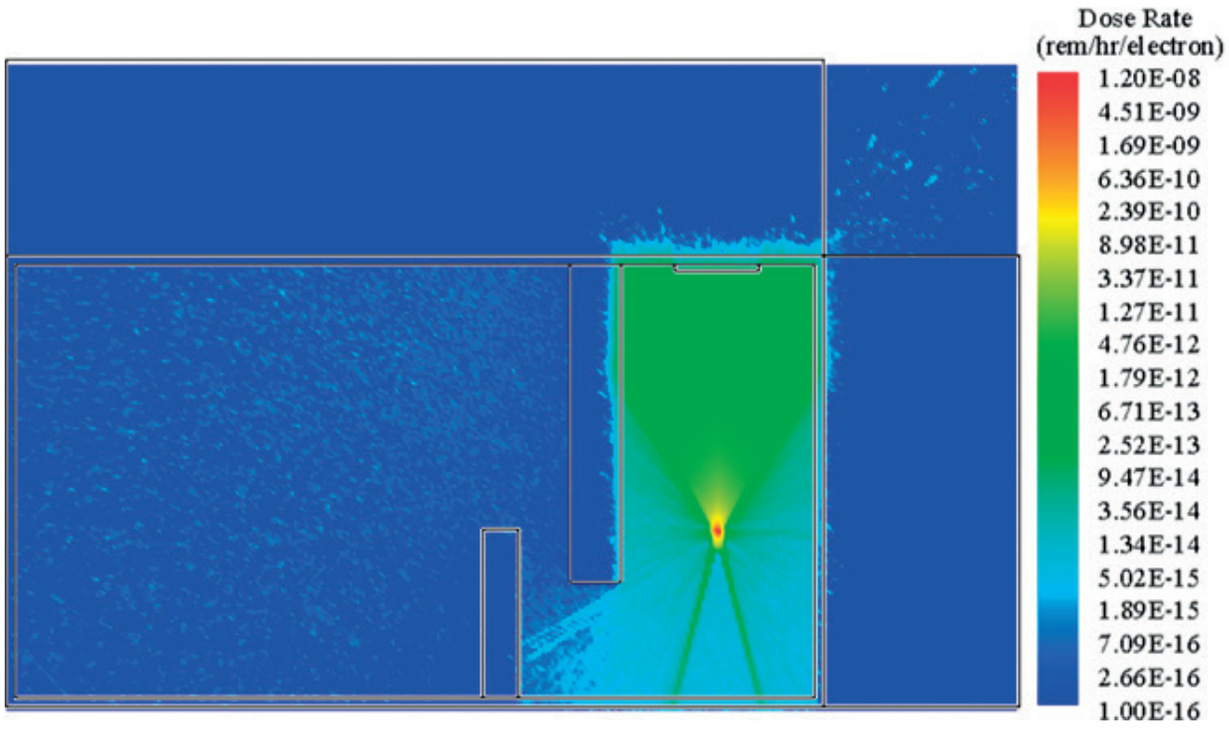

Figure 9. M6 linac in the 2nd configuration: dose rates for 3 MeV electron beam.

shielding and collimators results in an increase in the dose rates throughout the facility. When compared to the results from configurations 1 and 2, it was found that the dose rates in the accelerator bay to the rear and sides of the linac increased by an order of magnitude.

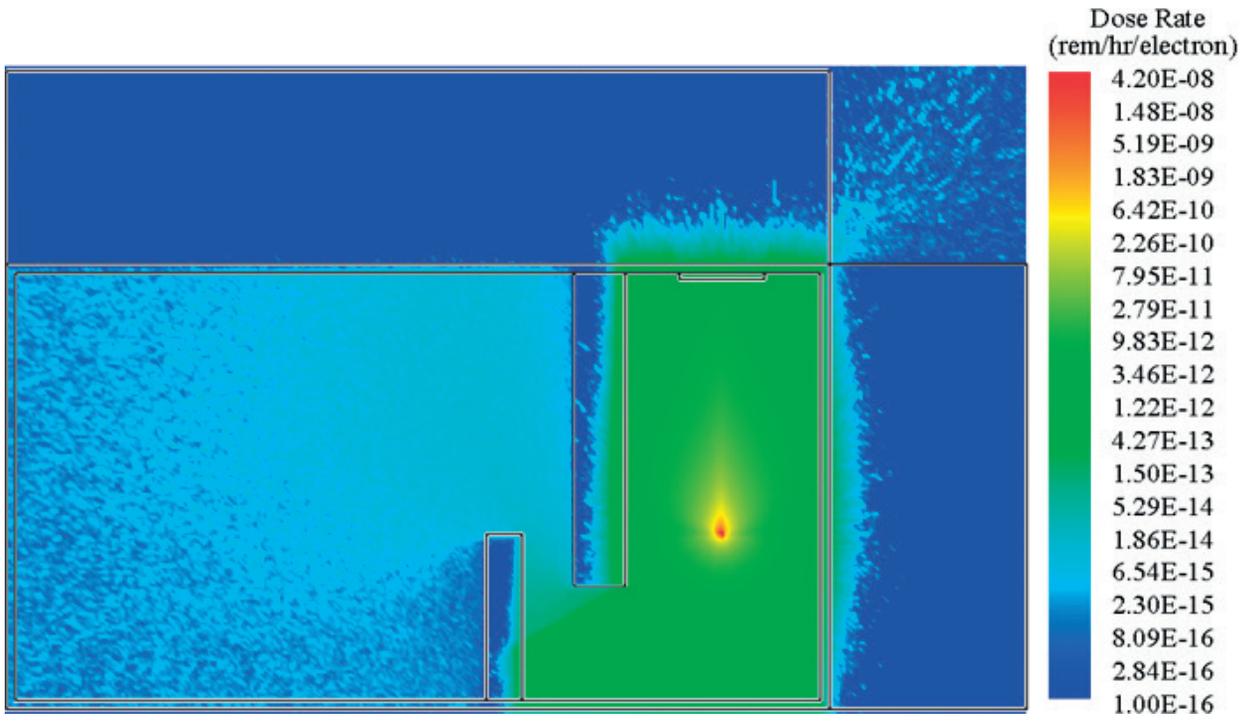

Figure 10. M6 linac without shielding and collimators: dose rates for 6 MeV electron beam.

This is due to the removal of the lead shielding in the rear of the M6 linac. In addition, the dose rates increased within the shielding maze (8.9 ± 0.05 rem/h) as well as the entry way (1.4 ± 0.005 rem/h). A summary of results detailing the product of the F5 dose rate

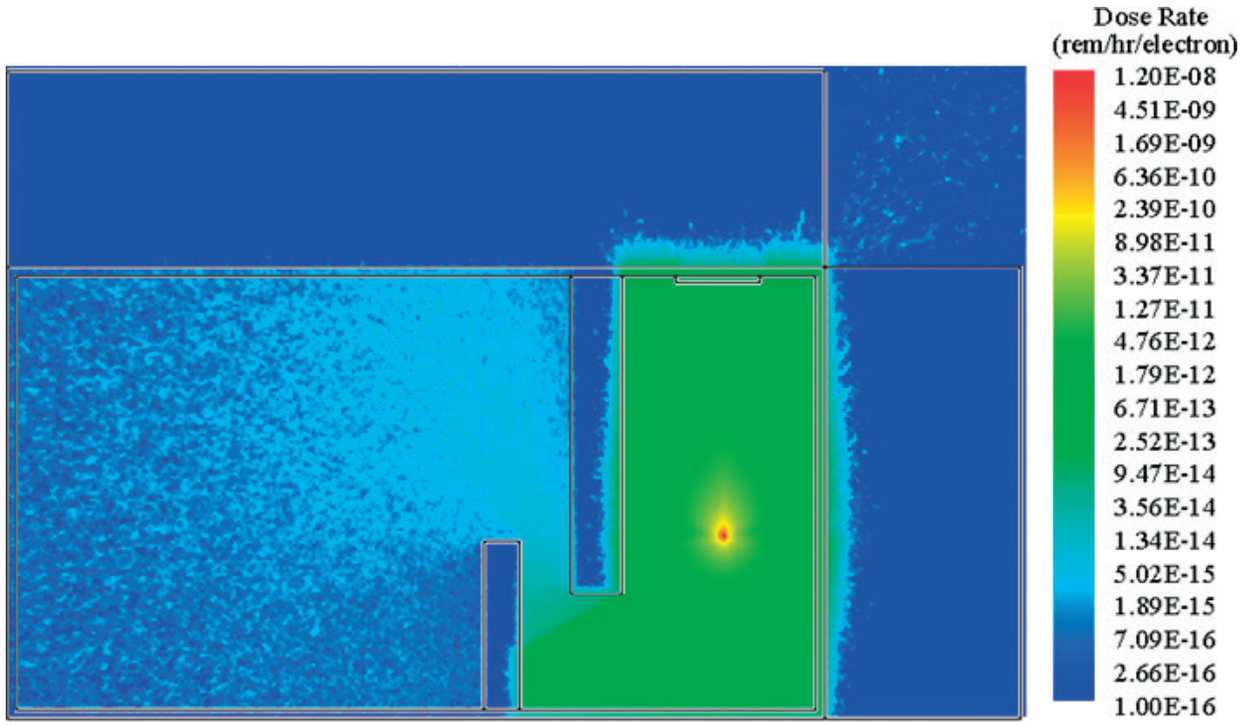

Figure 11. M6 linac without shielding and collimators: dose rates for 3 MeV electron beam.

tallies with the M6 electron current for all three configurations of the M6 linac operation is shown in **Table 2**. These results quantify the trends from the dose rate maps (shown in **Figures 6–11**) at specific building locations.

At all tally locations, the lowest dose rates occur under the normal M6 linac operation mode while the maximum dose rates occur when the collimators and shielding have been removed. When M6 collimators and shielding are present, the dose rates in the corners of the northern bay are reduced by a factor of 265 while the dose rates in the southern corners are reduced by a factor of 105. The entry way dose rates are reduced by a factor of 350 while the dose rate in the center of the shielding maze is reduced by a factor of 180. In the absence of the berm outside the northeast corner of the building, the dose rate was found to be under 3 rem/h. When the berm is present, the dose rates outside fall below the 10 Code of Federal Regulations (CFR) 20 limit, for the dose rate in an unrestricted area (2 m rem/h). At 2 m north of the linac, F5 tallies were used to determine the vertical dose rate profile for all three operating configurations (shown in **Figure 12**).

The results reflected large dose rates consistent with a fan beam shape at 1.2 m above the floor during normal operation. The use of collimators was shown to reduce the dose rates at all tally locations except at fan beam level. When collimators were removed, the fan beam expands to a cone shape and the dose rate increases. It was found that at dose rates near the ceiling (above 250 cm) were slightly lower (3.5×10^3 rem/h) due to the tally locations being outside the radiation cone beam. During operation of the M6 linac, the dose rate is continuously measured and monitored by an internal ion chamber calibrated to a distance of 1 m north of the linac. When the M6 linac was operated in the 6 MeV mode, the dose rate was measured to be 2.44×10^4 rem/h. The computational dose rate was determined by multiplying the normalized F5 tally result by the electron current and found to be 2.76×10^4 rem/h. The model and experimental measurement were found to be in agreement, with MCNP5 providing a conservative estimate for photon dose that is 1.13 time the measured value.

Facility location	Dose rate (rem/h)		
	Normal operation	Without collimators	Maximum doses
Entry room	0.0004 ± 0.00002	0.259 ± 0.0020	1.4 ± 0.005
Shielding maze	0.002 ± 0.0001	0.317 ± 0.0046	8.9 ± 0.05
Northern corners	3.29 ± 0.16	556 ± 1.3	583 ± 1.2
Southern corners	0.037 ± 0.0008	6.3 ± 0.07	206 ± 0.5
At 1 m	27,571 ± 69	42,081 ± 93	41,986 ± 88
Sample table	741 ± 1.93	1359 ± 2.7	1396 ± 2.8
Outside (no berm)	n/a	n/a	2.9 ± 0.08

Table 2. Accelerator facility dose rates caused by the M6 linac operation.

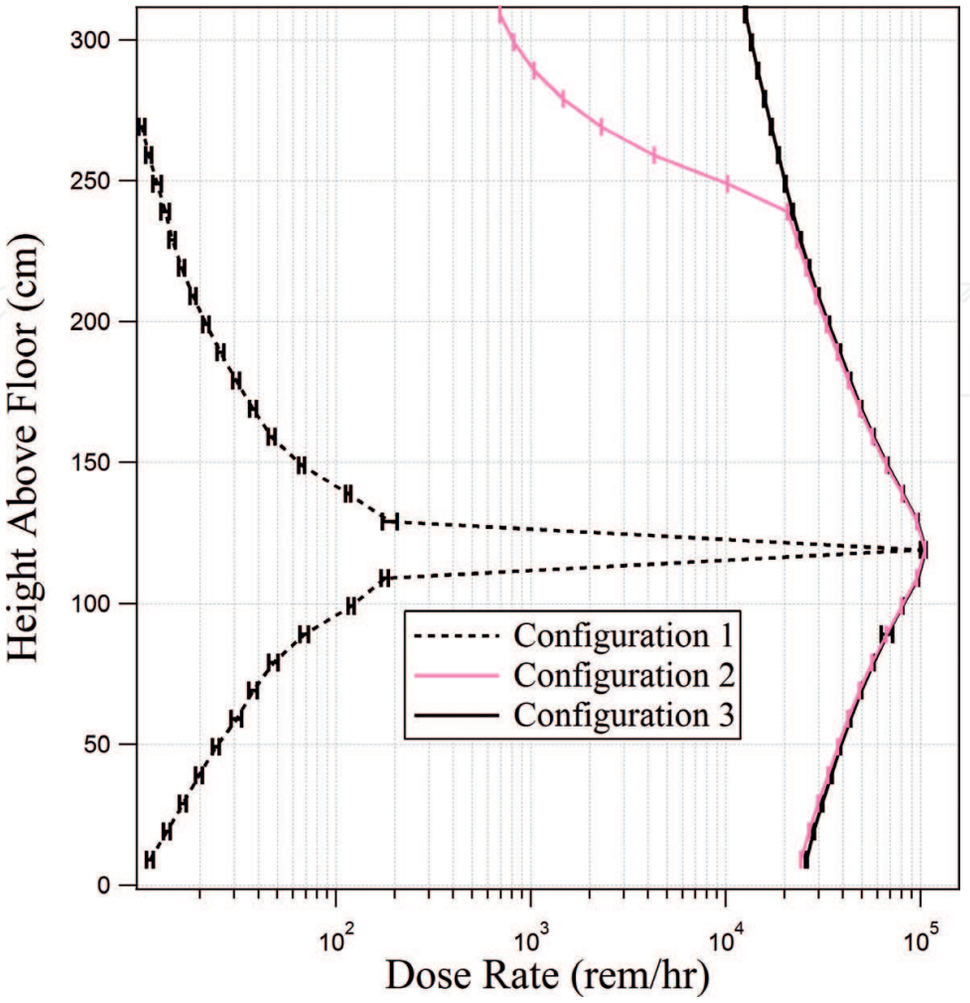

Figure 12. Vertical profile of dose rate during the M6 linac operation.

3.4. Radiation environment during operation of K15 linac

The K15 linac is not typically operated with a fan beam collimator, but rather with a 30° cone beam collimator. Other collimators may be used, but for the purpose of this study, the 30° cone case was considered. Two scenarios were modeled for the K15 linac operation: (1) normal operation with the cone collimator and shielding; (2) operation without shielding or collimators (the maximum dose rate scenario).

For each linac operating configuration, the TMESH/RMESH tally was used to determine the overall dose rate footprint in the building. Due to the energies of the photons generated in the linac target in the high energy mode being greater than the neutron binding energies of some materials in the linac shielding as well as the facility room structures, the photoneutron flux as well as its contribution to the dose rate must be considered. For photon energies higher than 10 MeV, photoneutron generation was expected. For example, photoneutron thresholds for isotopes in some materials are the following: 10.56 MeV for ^{14}N, 13.06 MeV for ^{27}Al, 10.23 MeV for ^{55}Mn, 11.20 MeV for ^{56}Fe, 12.22 MeV for ^{58}Ni, 10.85 MeV for ^{63}Cu, and 11.86 MeV for ^{64}Zn.

Under normal operation of the K15 linac, the photon dose rates were computed and shown in **Figures 13** and **14** for the low and high energy modes, respectively. The trends in the computed dose rates due to the K15 operation were found to be similar to those due to the M6 linac operation. The dose rates in the accelerator bay were highest, while the shielding maze helped to minimize dose rates in the entry way. The earthen berm minimized the photon dose rate outside of the facility to effectively nothing. Dose rates to the sides and rear of the K15 linac were higher when operated in high energy mode as compared to low energy mode. The vertical profile of the photon dose rate at 1 m north of the linac was measured using F5 tallies and is shown in **Figure 15**. The error associated with each value is less than the 5% recommended by MCNP for F5 tallies.

The computed normalized results show that the photon dose rate is largest down the axis of the collimated photon beam (9.5×10^{-8} rem/h/electron), at a height of 1.11 m above the floor. The dose rates near the floor (9.0×10^{-12} rem/h/electron) and the ceiling (1.0×10^{-8} rem/h/electron) of the building were determined to be approximately four orders of magnitude lower than the dose rate in the beam axis. The largest dose rates were found to occur between heights of 75 and 125 cm, corresponding to the height of the conical collimated photon beam. Dose rates quickly decrease outside of the photon beam.

The neutron contribution to the dose rate during the normal K15 linac operation in the high energy mode is shown in **Figure 16**. No photoneutrons were produced during operation of the K15 linac in the low energy mode due to the endpoint energy of the bremsstrahlung being below the (γ,n) reaction thresholds of the materials in the MCNPX model.

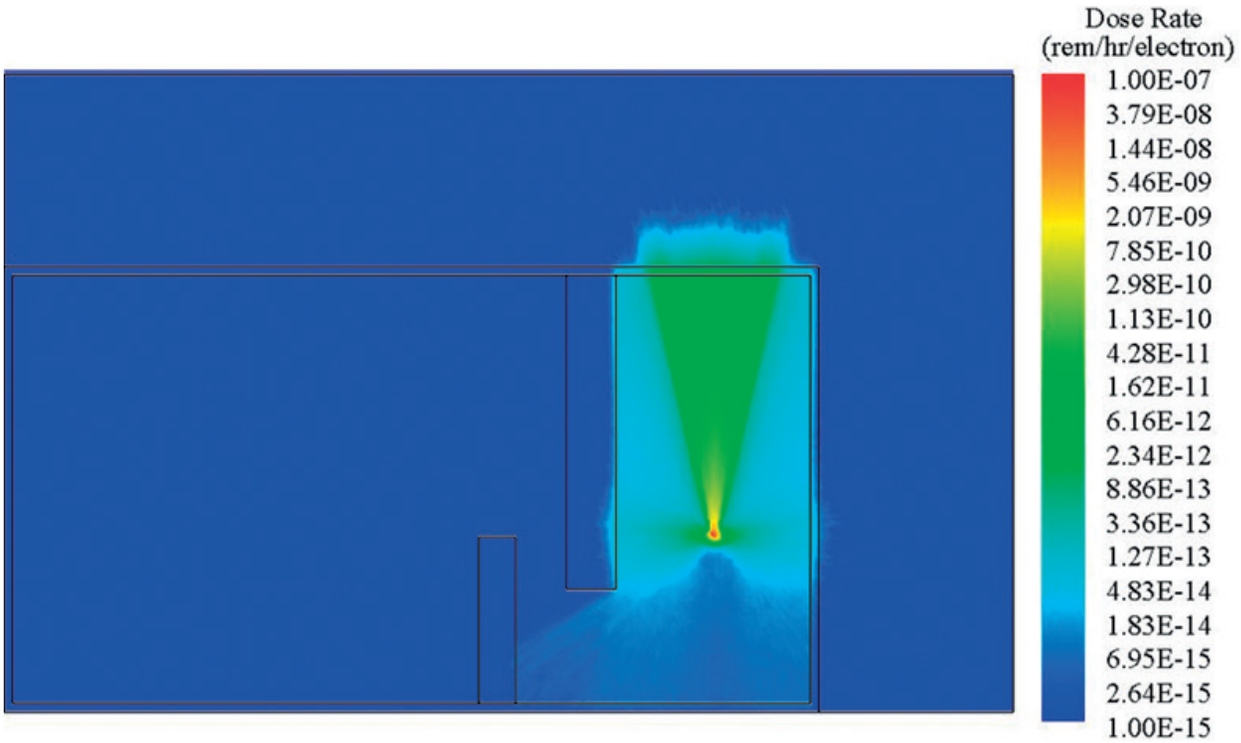

Figure 13. K15 linac in configuration 1: photon dose rates for 9 MeV electron beam.

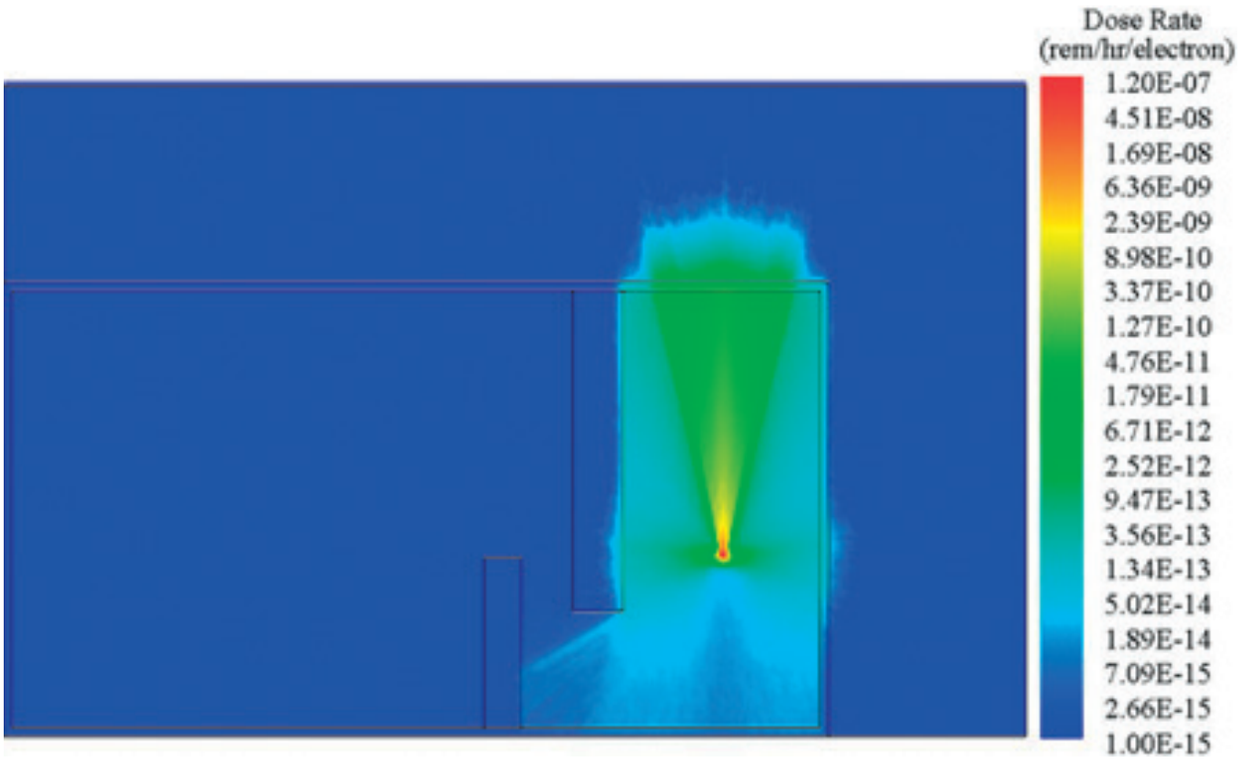

Figure 14. K15 linac in configuration 1: photon dose rates for 15 MeV electron beam.

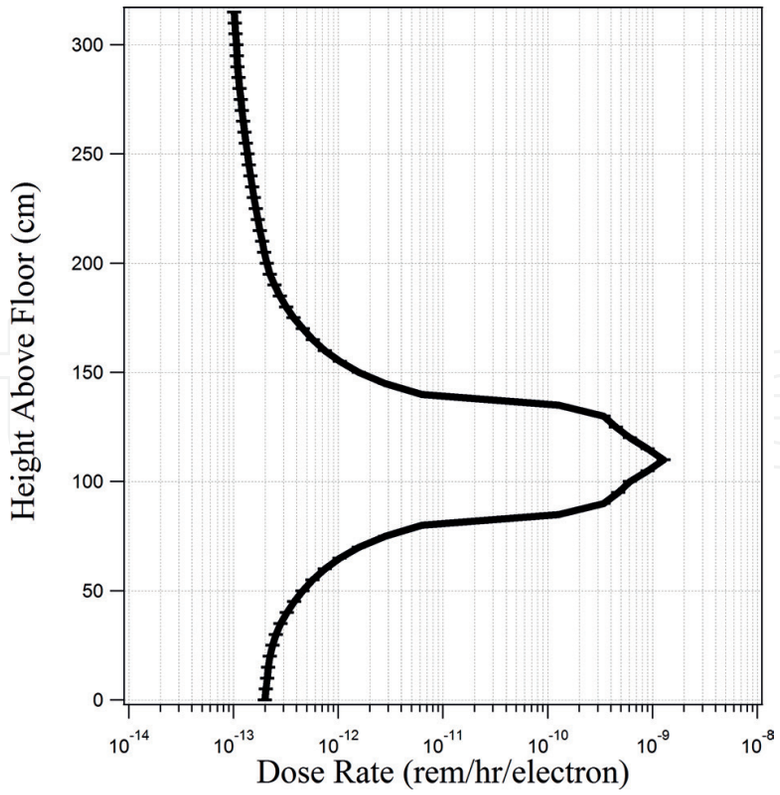

Figure 15. Vertical profile of photon dose rate in normal operation of K15 linac in high energy mode.

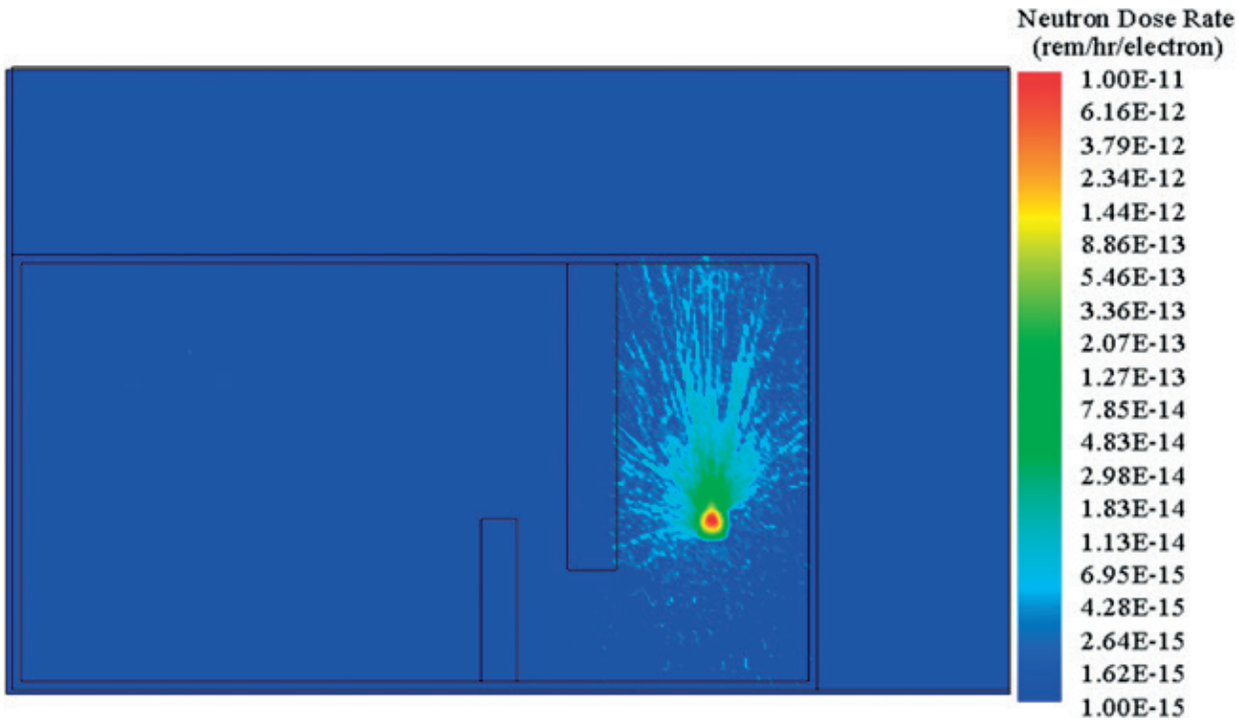

Figure 16. K15 linac in configuration 1: neutron dose rates for 15 MeV electron beam.

The results show that the neutron flux was primarily contained within the accelerator bay. Neutron contribution to dose rate was highest north of the linac primarily due to the lack of low-Z shielding behind the target head. The back end of the K15 linac contained several inches of polyethylene shielding which reduced the neutron dose rate in the southern end of the bay. The maximum dose rate due to neutron flux was determined to be several orders of magnitude lower than the photon contribution. While the profile shape of the photon dose rate corresponded to the shape of the conic collimator, the neutron dose rate does not possess the same shape. This is because neutrons were produced in the high-Z collimator materials rather than being shaped by it. The neutron spectrum at a distance of 1 m behind of the linac target was computed using an F5 tally (see **Figure 17**). The largest flux of neutrons was determined to be in the 0.1–1 MeV range with the second largest flux for neutrons just above the thermal range (10^{-8}–10^{-7} MeV). The total neutron flux at the F5 tally location was found to be 4.8×10^4 neutrons/cm^2/s.

The geometry in the MCNPX model was modified to simulate the K15 linac operation without shielding and collimators in order to determine the maximum dose rate due to operation of the linac in the high energy mode. Maximum photon dose rate results are shown in **Figure 18**. The results show that without collimators and shielding, the dose rates due to photons increase throughout the building. Comparing the RMESH tally data between the two linac operating configurations reveals that the K15 collimator and shielding materials help to reduce photon dose rates by factors of 238, 33 and 7.5 times for locations at 1 m north of the linac, in the center of the shielding maze and in the center of the entryway, respectively.

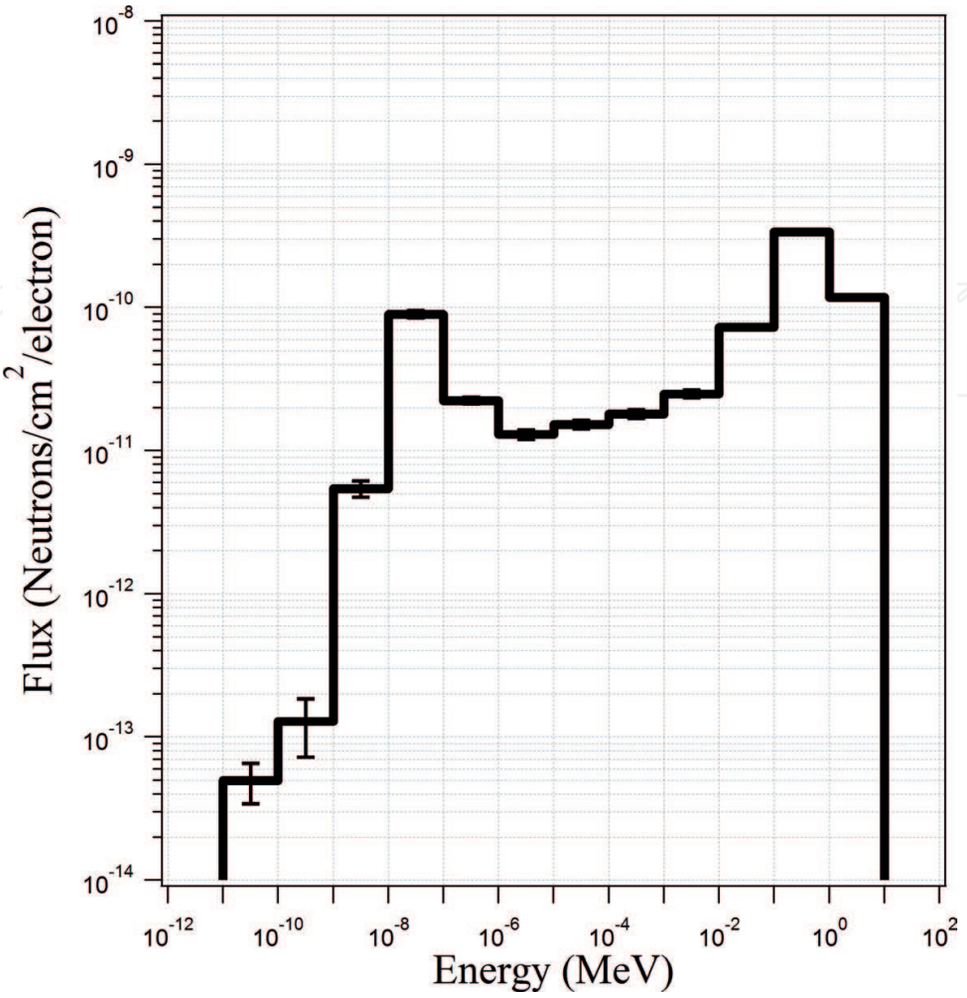

Figure 17. Photoneutron spectrum at 1 m from the K15 linac target.

The maximum neutron dose rate footprint is similar to that of the normal neutron dose rate map with the exception that the dose rate has increased in the southern half of the accelerator bay. This is due to the fact that the polyethylene neutron shielding was removed in the rear of the linac.

The photon dose rate from the K15 linac was experimentally measured at Varian Medical Systems by an internal ion chamber (calibrated at 1 m north of the linac) and found to be 11,700 rem/min for high energy mode and 3500 rem/min for low energy mode. MCNPX F5 tally results at the same locations yielded values of 1.40×10^{-9} and 3.10×10^{-10} rem/h/starting electron for high and low energy respectively. Multiplying these tally values by the respective DC averaged electron currents and converting to the appropriate time scale provided values for high and low energy dose rate as 15,744 and 3687 rem/min, respectively. Thus, the MCNPX model provided conservative estimates of photon dose rate by scale factors of 1.35 for the high energy mode and 1.05 for the low energy mode.

It is important for safety purposes to evaluate differences in the radiation production between the two linacs that can be used at the same facility. At 1 m north of the linac, the M6 linac generates a photon dose rate of over 400 rem/min. At the same location, the photons from the K15 linac generate dose rates 28 times larger (high energy mode) and 8 times larger (low energy

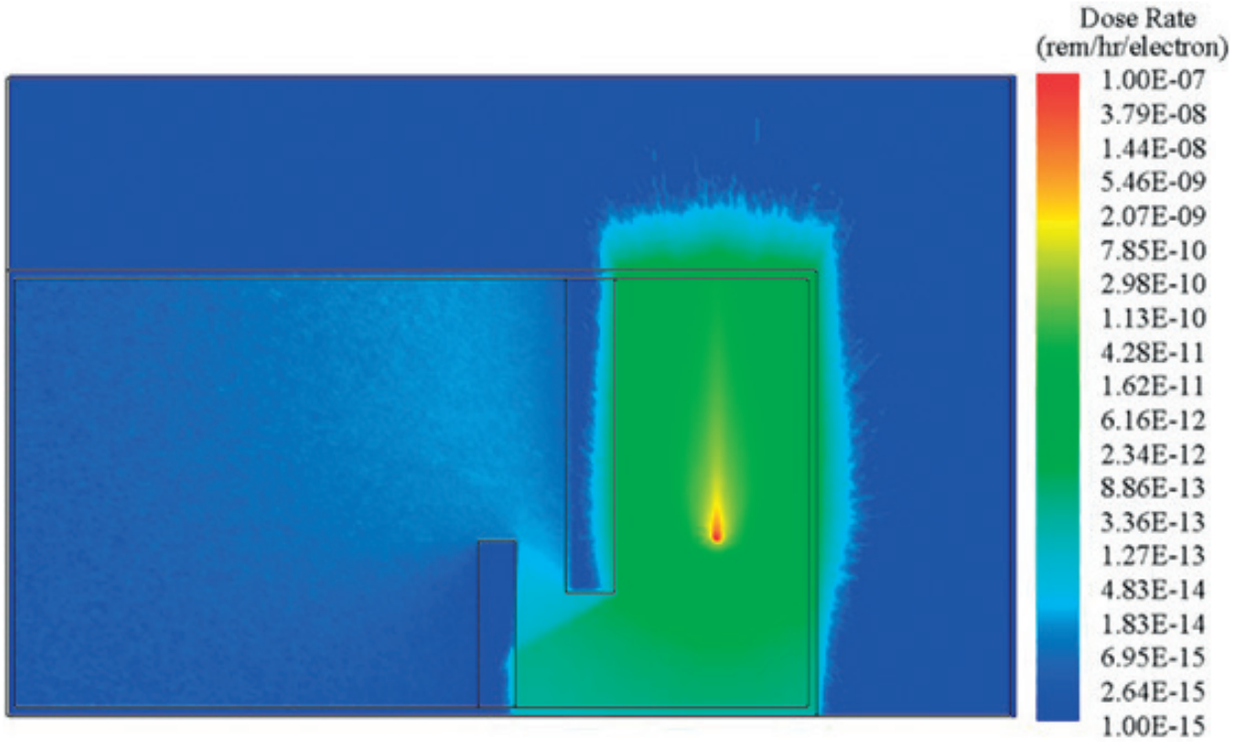

Figure 18. K15 linac without shielding and collimators: photon dose rate for 15 MeV electron beam.

mode) than the M6 linac does. When compared to the M6 results, the K15 maximum dose rates an order of magnitude larger. At 1 cm behind the respective linac targets, the maximum photon flux occurs within a 10° conic angle. At this angle, the total photon flux (normalized computational result multiplied by the electron current) of the K15 linac in the high energy mode is over four times as large as that of the M6 linac (**Table 3**).

Linac model (Electron energy)	**K15 (15 MeV)**	**K15 (9 MeV)**	**M6 (6 MeV)**
	Photon Flux (photons/cm²/s)		
Angle, degrees			
10	4.27E + 14	1.47E + 14	9.53E + 13
20	2.81E + 14	1.07E + 14	7.00E + 13
30	1.89E + 14	7.66E + 13	4.93E + 13
40	1.27E + 14	5.42E + 13	3.40E + 13
50	8.03E + 13	3.61E + 13	2.19E + 13
60	4.38E + 13	2.09E + 13	1.24E + 13
70	1.78E + 13	8.97E + 12	5.41E + 12
80	4.34E + 12	2.60E + 12	1.29E + 12
90	9.75E + 10	6.91E + 10	2.04E + 10

Linac model (Electron energy)	K15 (15 MeV)	K15 (9 MeV)	M6 (6 MeV)
	Does Rate (rem/m/min)		
Measured dose rate	11,700	3500	406.67
MCNP computed dose rate	15,744	3687	460
Scale factor (MCNP dose/measured dose)	1.35	1.05	1.13

Table 3. Characteristics of M6 and K15 linacs.

4. Conclusion

Radiation safety aspects of operation of electron linacs equipped with bremsstrahlung converters were studied. The operation of Varian linacs M6 (3 and 6 MeV electron beams) and K15 (9 and 15 MeV electron beams) at the accelerator facility of University of Nevada, Las Vegas was investigated. High-energy photon and photoneutron production during the linac operation were analyzed using Monte Carlo computational models. The bremsstrahlung spectral and angular distributions were computationally determined for the M6 linac and the K15 linac. Biological equivalent dose rates due to accelerator operation were evaluated using the flux-to-dose conversion factors. Dose rates were computed for the accelerator facility for the linac use under different operating conditions. The results showed that the use of collimators and the linac's internal shielding significantly reduced the dose rates throughout the facility. Measurements shown that computational models allow conservative dose rate estimations.

Photoneutron dose rates within the facility were computed for the K15 linac in the high energy mode. While the largest neutron contribution to dose rate was four orders of magnitude lower than the photon contribution, it was still large enough to warrant consideration when designing the bunker shielding.

Author details

Matthew Hodges* and Alexander Barzilov

*Address all correspondence to: Hodgesm@unlv.nevada.edu

University of Nevada, Las Vegas, United States

References

[1] Wangler T. RF Linear Accelerators. 2nd ed. Weinheim: Wiley-VCH Verlag; 2008. 466 p. DOI: 10.1002/9783527623426

[2] Broemme J et al. Adjuvant therapy after resection of brain metastases: Frameless image-guided LINAC-based radiosurgery and stereotactic hypofractionated radiotherapy. Strahlentherapie und Onkologie. 2013;**189**(9):765-770. DOI: 10.1007/s00066-013-0409-z

[3] Fong BM et al. Hearing preservation after LINAC radiosurgery and LINAC radiotherapy for vestibular Schwannoma. Journal of Clinical Neuroscience. 2012;**19**:1065-1070. DOI: 10.1016/j.jocn.2012.01.015

[4] Brice S. Proton improvement plan II: An 800 MeV superconducting linac to support megawatt proton beams at Fermilab. Nuclear and Particle Physics Proceedings. 2016;**273-275**:238-243. DOI: 10.1016/j.nuclphysbps.2015.09.032

[5] Brunner O et al. Assessment of the basic parameters of the CERN superconducting proton linac. Physical Review Special Topics - Accelerators and Beams. 2009;**12**:070402-1-070402-24. DOI: 10.1103/PhysRevSTAB.12.070402

[6] Kim HJ et al. Superconducting linac for the rare isotope science project. Journal of the Korean Physical Society. 2015;**66**(3):413-418. DOI: 10.3938/jkps.66.413

[7] Jones J et al. Detection of shielded nuclear material in a cargo container. Nuclear Instruments and Methods in Physics Research A. 2006;**562**:1085-1088. DOI: 10.1016/j.nima.2006.02.101

[8] Barzilov A, Womble PC, Vourvopoulos G. NELIS – A neutron inspection system for detection of illicit drugs. AIP Conference Proceedings. 2003;**680**:939-942. DOI: 10.1063/1.1619863

[9] Chen G, Bennett G, Perticone D. Dual-energy X-ray radiography for automatic high-Z material detection. Nuclear Instruments and Methods in Physics Research B. 2007;**261**:356-359. DOI: 10.1016/j.nimb.2007.04.036

[10] Hartman J et al. 3D imaging using combined neutron-photon fan-beam tomography: A Monte Carlo study. Applied Radiation and Isotopes. 2016;**111**:119-116. DOI: 10.1016/j.apradiso.2016.02.018

[11] Kosako K et al. Angular distributions of Photoneutrons from copper and tungsten targets bombarded by 18, 28, and 38 MeV electrons. Journal of Nuclear Science and Technology. 2011;**48**(2):227-236. DOI: 10.1080/18811248.2011.9711696

[12] U.S. NRC. Units of Radiation Dose [Internet]. 2017. Available from: http://www.nrc.gov/reading-rm/doc-collections/cfr/part020/part020-1004.html [Accessed: Aug 25, 2017]

[13] ANSI Standard ANSI/ANS 6.1.1-1977. Neutron and Gamma-ray Flux-to-Dose-Rate Factors. La Grange, Illinois: American Nuclear Society; 1977

[14] Kirkby C et al. RBE of KV CBCT radiation determined by Monte Carlo DNA damage simulations. Physics in Medicine and Biology. 2013;**58**(16):5693-5704. DOI: 10.1088/0031-9155/58/16/5693

[15] Heerikhuisen J, Florinski V, Zank GP. Interaction between the solar wind and interstellar gas: a comparison between Monte Carlo and fluid approaches. Journal of Geophysics Research: Atmosphere. 2006;**111**(A6):1-8. DOI: 10.1029/2006JA011604

[16] Creal D. A survey of sequential Monte Carlo methods for economics and finance. Economic Review. 2012;**31**(3):245-296. DOI: 10.1080/07474938.2011.607333

[17] Barzilov A, Novikov I, Cooper B. Computational study of pulsed neutron induced activation analysis of cargo. Journal of Radioanalytical and Nuclear Chemistry. 2009;**282**:177-181. DOI: 10.1007/s10967-009-0298-x

[18] Barzilov A, Womble PC. Study of Doppler broadening of gamma-ray spectra in 14-MeV neutron activation analysis. Journal of Radioanalytical and Nuclear Chemistry. 2014;**301**:811-819. DOI: 10.1007/s10967-014-3189-8

[19] Brown F, Kiedrowski B, Bull J. MCNP5 1.60 Release Notes. Los Alamos National Laboratory. Los Alamos, New Mexico: LA-UR-10-06235; 2010

[20] Pelowitz D. MCNPX 2.7.0 Extensions. Los Alamos National Laboratory. Los Alamos, New Mexico. LA-UR-11-02295; 2011

[21] McConn RJ et al. Compendium of Material Composition Data for Radiation Transport Modeling. Richland, Washington: Pacific Northwest National Laboratory. PNNL-15780; 2011

[22] Verbeke J et al. Simulation of Neutron and Gamma Ray Emission from Fission and Photofission. Livermore, California: Lawrence Livermore National Laboratory. UCRL-AR-228518; 2014

[23] Hughes HG. Treating Electron Transport in MCNP. Los Alamos National Laboratory. Los Alamos, New Mexico: LA-UR-96-4583; 1997